Available online at www.sciencedirect.com
ScienceDirect
Journal of Computational Physics 227 (2008) 3738–3757
JOURNAL OF COMPUTATIONAL PHYSICS
www.elsevier.com/locate/jcp

A piecewise linear finite element discretization of the diffusion equation for arbitrary polyhedral grids

Teresa S. Bailey [a], Marvin L. Adams [a,*], Brian Yang [b], Michael R. Zika [b]

[a] *Texas A&M University, Department of Nuclear Engineering, College Station, TX 77843-3133, United States*
[b] *Lawrence Livermore National Laboratory, Livermore, CA 94551, United States*

Received 10 February 2007; received in revised form 26 October 2007; accepted 12 November 2007
Available online 3 December 2007

Abstract

We develop a piecewise linear (PWL) Galerkin finite element spatial discretization for the multi-dimensional radiation diffusion equation. It uses recently introduced piecewise linear weight and basis functions in the finite element approximation and it can be applied on arbitrary polygonal (2D) or polyhedral (3D) grids. We first demonstrate some analytical properties of the PWL method and perform a simple mode analysis to compare the PWL method with Palmer's vertex-centered finite-volume method and with a bilinear continuous finite element method. We then show that this new PWL method gives solutions comparable to those from Palmer's. However, since the PWL method produces a symmetric positive-definite coefficient matrix, it should be substantially more computationally efficient than Palmer's method, which produces an asymmetric matrix. We conclude that the Galerkin PWL method is an attractive option for solving diffusion equations on unstructured grids.

Keywords: Diffusion; Arbitrary polyhedral grids; Piecewise linear; Finite element; Finite-volume; Unstructured grids; Adaptive mesh refinement

1. Introduction

Several methods have been developed to solve the radiation diffusion equation on arbitrary polyhedral (3D) and polygonal (2D) meshes. A vertex-centered finite-volume (FV) method developed by Palmer [1,2] divides each cell into "corner" subcells and enforces conservation on each dual cell, where a dual cell is the union of corners that touch a vertex. This method is second-order accurate, with relatively small error norms, and is exact on any grid if the exact solution is linear in the position variables. However, Palmer's method does not generate a symmetric coefficient matrix, so the matrix system is (relatively) computationally expensive to store and solve. Wachspress previously developed rational–polynomial basis functions [3] that can be

* Corresponding author. Tel.: +1 979 845 4198; fax: +1 979 845 6443.
E-mail addresses: baileyte@tamu.edu (T.S. Bailey), mladams@tamu.edu (M.L. Adams), tbyang@llnl.gov (B. Yang), zika@llnl.gov (M.R. Zika).

0021-9991/$ - see front matter © 2007 Elsevier Inc. All rights reserved.
doi:10.1016/j.jcp.2007.11.026

applied to polyhedral cells in a finite element method (FEM). His functions have the advantage that a Galerkin FEM formulation will yield a symmetric positive-definite (SPD) matrix, but the disadvantage that the basis function integrals must be done numerically [4].

In this work, we apply a relatively new FEM basis function – the "PieceWise Linear" (PWL) function [5] – to the radiation diffusion equation on arbitrary polygonal and polyhedral meshes. (Throughout this paper we generalize the term "polyhedra" to include cells whose faces are not planar and thus are not polyhedral by the usual definition. We discuss this further in Appendix, including a description of how we handle non-planar faces.) The goals of our PWL work are to gain an SPD coefficient matrix, retain the simplicity and accuracy of Palmer's finite-volume method, and avoid the numerical integrations that plague Wachspress's method. As part of our development we show that in most cases Palmer's method is, in fact, a FEM with PWL basis functions, but with Petrov–Galerkin weighting. (The weight functions are constants over dual cells.) We then show that the PWL method produces a well-posed discrete problem, and we show that the PWL method will have second-order convergence properties. To further characterize the methods we have performed a simple mode analysis on the lumped and unlumped PWL methods, Palmer's method, and the lumped and unlumped bilinear continuous finite element methods (BLC). We compare our Galerkin PWL method against Palmer's method on multiple test problems. We find that our method meets all of our goals: it yields accuracy comparable to Palmer's method, produces an SPD matrix, and involves only very simple integrations.

We remark that this is an active field of research, with methods constantly under development. For example, Morel has proposed a cell-centered FV method for polyhedral cells [6], and support-operator methods have been proposed by Kuznetsov et al. [7]. We do not claim that our PWL FEM is superior to these methods for all problems. Further research is needed to determine which methods are best for different applications.

2. Development

2.1. Introduction

An asymptotic limit of the radiation transport equation is a time-dependent radiation conservation equation [8]:

$$a\frac{\partial}{\partial t}(T(\vec{r},t))^4 - \vec{\nabla}\cdot\frac{ac}{3\sigma_R}\vec{\nabla}(T(\vec{r},t))^4 = Q(\vec{r},t). \tag{1}$$

For simplicity we express Eq. (1) as

$$\frac{1}{c}\frac{\partial}{\partial t}E(\vec{r},t) - \vec{\nabla}\cdot D\vec{\nabla}E(\vec{r},t) = Q(\vec{r},t) \tag{2}$$

where E is the radiation energy density, Q is the source, and D is a diffusion coefficient. We begin discretizing Eq. (2) by applying a simple fully implicit Euler approximation to the time derivative, which results in

$$\frac{1}{c}\frac{(E^{n+1}(\vec{r}) - E^n(\vec{r}))}{\Delta t} - \vec{\nabla}\cdot D\vec{\nabla}E^{n+1}(\vec{r}) = Q^{n+1}(\vec{r}), \tag{3}$$

where the n superscripts represent the time step index. In Eq. (3), we solve for E^{n+1} to obtain a diffusion equation

$$-\vec{\nabla}\cdot D\vec{\nabla}E^{n+1}(\vec{r}) + \sigma E^{n+1}(\vec{r}) = S^{n+1}(\vec{r}), \tag{4}$$

where

$$\sigma = \frac{1}{c\Delta t} \tag{5}$$

and

$$S^{n+1}(\vec{r}) = Q^{n+1}(\vec{r}) + \frac{1}{c\Delta t}E^n(\vec{r}). \tag{6}$$

Eq. (4) is the final form of the steady state diffusion equation to which we will apply all spatial discretizations. We also define the net current vector:

$$\vec{F} = -D\vec{\nabla}E. \tag{7}$$

2.2. Galerkin PWL FEM

To apply an FEM to the diffusion equation, we first multiply the equation by a weight function and integrate it over the problem domain. If the ith weight function is non-zero only on cells that touch the ith vertex, then we have

$$\int_{z\,\text{at}\,i} \mathrm{d}^3 r w_i(\vec{r})[-\vec{\nabla}\cdot D\vec{\nabla}E(\vec{r}) + \sigma E(\vec{r}) - S(\vec{r})] = 0, \tag{8}$$

where z denotes cells (which we sometimes call "zones"). The divergence theorem produces:

$$\int_{\partial z\,\text{at}\,i} \mathrm{d}^2 r w_i(\vec{r})\vec{n}\cdot\vec{F} + \int_{z\,\text{at}\,i} \mathrm{d}^3 r[D\vec{\nabla}E(\vec{r})\cdot\vec{\nabla}w_i(\vec{r}) + w_i(\vec{r})(\sigma E(\vec{r}) - S(\vec{r}))] = 0. \tag{9}$$

The first term is zero if the cells over which the equation is integrated are not on the boundary of the domain. We ignore it in the remainder of this development. An approximation can be made for E in terms of known basis functions:

$$E(\vec{r}) = \sum\nolimits_{\text{all}\,j} E_j b_j(\vec{r}), \tag{10}$$

which results in

$$\sum_j E_j \left\{ \int_{z\,\text{at}\,i} \mathrm{d}^3 r[D\vec{\nabla}b_j(\vec{r})\cdot\vec{\nabla}w_i(\vec{r}) + \sigma b_j(\vec{r})w_i(\vec{r})] \right\} = \int_{z\,\text{at}\,i} \mathrm{d}^3 r w_i(\vec{r})S(\vec{r}). \tag{11}$$

Eq. (11) is N equations for N unknowns. Given our assumption of one weight function per vertex, N is the number of vertices in the mesh.

A Galerkin FEM sets $w_i = b_i$. It is not difficult to show that this yields a symmetric positive-definite matrix. In this work we develop a Galerkin FEM that employs the piecewise linear (PWL) weight and basis functions developed recently by Stone and Adams [5]. In the development of vertex-centered methods for arbitrary polyhedral cells, each polyhedral cell is divided into subcell volumes called sides, corners and wedges. A side is a tetrahedron made from two adjacent vertices, the zone center and a face center. A corner, which will be used primarily in the development of Palmer's vertex-centered finite-volume method, is defined as the union of all half-sides that touch a vertex in one zone. A wedge is defined to be a half-side. See Figs. 1–3 for depictions of side subcells, corner subcells, and wedges in a hexahedral cell.

The PWL function centered at vertex j can be written in three-dimensions as

$$b_j(\vec{r}) = t_j(\vec{r}) + \sum_{\text{faces at}\,j} \beta_{f,j} t_{\text{f}}(\vec{r}) + \alpha_{z,j} t_{\text{z}}(\vec{r}), \tag{12}$$

where the t functions are standard linear functions defined tetrahedron by tetrahedron. For example, t_j equals 1 at the jth vertex and decreases linearly to zero at all other vertices of each side that touches point j. t_{z} is unity

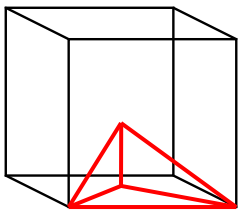

Fig. 1. Side in a hexahedral cell.

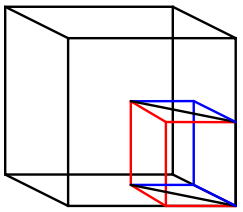

Fig. 2. Corner in a hexahedral cell.

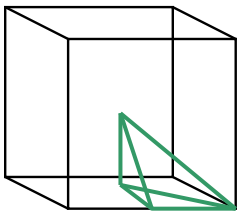

Fig. 3. Wedge in a hexahedral cell.

at the cell midpoint and zero at each face midpoint and each cell vertex. t_{f} is unity at the face midpoint and zero at the cell midpoint and at each of the face's vertices. The α_{z} and β_{f} are weights that give the cell and face midpoints as weighted averages of their vertices:

$$\vec{r}_{\mathrm{z}} \equiv \text{cell midpoint} = \sum_{j\,\text{at}\,z} \alpha_{z,j}\vec{r}_j; \tag{13}$$

$$\vec{r}_{\mathrm{f}} \equiv \text{face midpoint} = \sum_{j\,\text{at}\,f} \beta_{f,j}\vec{r}_j. \tag{14}$$

Each basis function is piecewise linear on each side, which makes integration over sides straightforward. (Note that the gradient of a basis function is constant on a side.) Fig. 4 shows a plot of a PWL basis function for a two-dimensional rectangular cell.

The definitions in Eqs. (12)–(14) guarantee that any linear function of (x, y, z) can be exactly represented as an expansion in these basis functions. (This subtlety is what makes the method work. Effectively, the functions

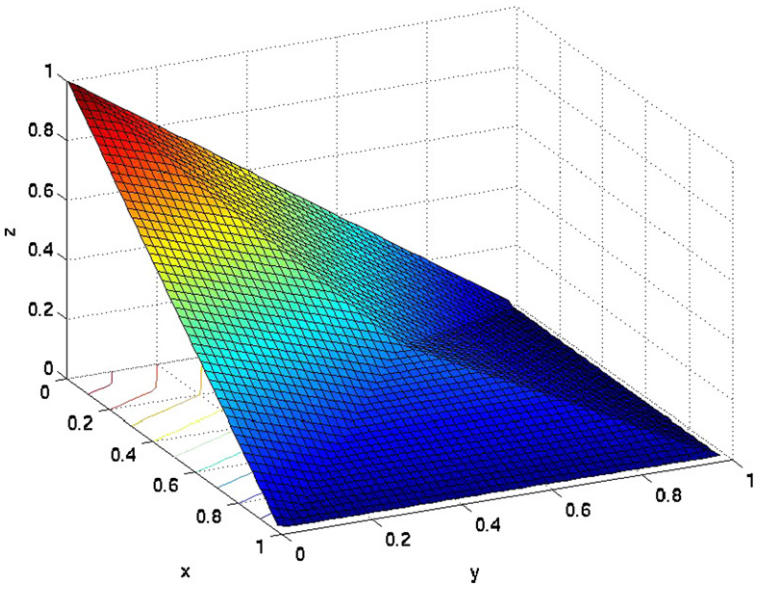

Fig. 4. 2D piecewise linear basis functions.

generate interpolated values at cell and face midpoints, in such a way that the interpolated values are perfect for linear functions.)

Our Galerkin FEM uses PWL functions for the w and b in the general equation above, with one exception: we *lump* the "mass matrix." That is, we make the replacement

$$\int_{z \text{ at } i} \mathrm{d}^3 r[\sigma b_j(r) w_i(r)] \underset{\text{lump}}{\rightarrow} \delta_{ij} \int_{c \text{ at } i} \mathrm{d}^3 r[\sigma], \tag{15}$$

where c refers to a "corner" subcell. On orthogonal grids with σ constant in each cell, this is equivalent to standard FEM mass-matrix lumping, because the volume of the corner at each vertex and the integral of the weight function over the cell both equal 1/8 of the cell volume (or 1/4 of the cell area in 2D). On general grids, however, Eq. (15) is not equivalent to standard mass-matrix lumping. We choose this non-standard lumping so that our source and collision terms are identical to those in Palmer's method, thus allowing our study to focus on different treatments of the diffusion term.

This completes the definition of our new method (except for boundary conditions, which are straightforward).

2.3. Palmer's vertex-centered finite-volume method

Palmer's method is developed by dividing each cell into corners, defining dual cells to be the union of corners at each vertex, and enforcing conservation over these dual cells. The gradient of the scalar flux is taken to be constant within each wedge subcell, and the cell-center scalar flux is an interpolant of the vertex scalar fluxes, defined such that it is exact for functions that are linear in x, y and z. The method enforces continuity of particle flow (the normal component of the current) across each dual cell boundary. See Refs. [1,2] for more details.

It is interesting to note that in most cases Palmer's FV method is equivalent to a Petrov–Galerkin FEM with PWL basis functions, with the mass-matrix lumping defined above, and with a constant diffusion coefficient in each side subcell volume. The weight functions for this case are given by

$$w_i(\vec{r}) = \begin{cases} 1, & \vec{r} \in \text{any corner that touches vertex } i, \\ 0, & \text{otherwise.} \end{cases} \tag{16}$$

As far as we know, this has not been previously observed. This illuminates the close connection between Palmer's method and our Galerkin FEM, and it also may permit Palmer's method to be better understood and analyzed. The exceptions to this interpretation occur when the diffusion coefficient, D, is allowed to vary within a cell. In such cases, Palmer's method does not assume that E varies linearly within each side, but instead allows E's slope to change so that $\vec{n} \cdot D\vec{\nabla}E$ is the same in both wedges where they meet inside one side.

Both methods should be exact (within the limits of roundoff error) if the solution is a linear function of x, y and z, regardless of how distorted the spatial cells become. (We test this below.) This follows from the construction of the PWL basis functions.

3. Analyses of PWL and related methods

3.1. Well-posedness

Using the Lax-Milgram Lemma, we can show that the PWL discretization of the diffusion equation results in a well-posed discrete problem. This discrete problem is derived from the weak formulation of the diffusion equation:

$$\int_\Omega \mathrm{d}\Omega \vec{\nabla} v \cdot \vec{\nabla} u + \lambda \int_\Omega \mathrm{d}\Omega v u = \int_\Omega \mathrm{d}\Omega v f, \quad u \in H_0^1(\Omega) \quad \text{and} \quad \forall v \in H_0^1(\Omega), \tag{17}$$

where $H_0^1(\Omega)$ is a Hilbert space with the norm:

$$\|w\|_{H_0^1(\Omega)} = (\|\nabla w\|_{L^2}^2 + \|w\|_{L^2}^2)^{1/2}. \tag{18}$$

Here λ plays the role of σ/D. Also for simplicity, define

$$\begin{aligned} a(u,v) &\equiv \int_\Omega \mathrm{d}\Omega \vec{\nabla} v \cdot \vec{\nabla} u + \lambda \int_\Omega \mathrm{d}\Omega v u, \\ S(v) &\equiv \int_\Omega \mathrm{d}\Omega v f. \end{aligned} \tag{19}$$

The Lax-Milgram lemma [9] states that a problem is well-posed (a solution exists and is unique) if

1. the weight and basis (or test and trial) functions are in a Hilbert space, H,
2. $a(u,v)$ is a bilinear form on H,
3. $a(u,v)$ is bounded,
4. $a(u,u)$ is coercive,
5. $S(v)$ is linear and bounded.

The first two elements of the lemma are obviously satisfied. To prove the third element, we start by taking the absolute value of $a(u,v)$ and writing the integrals in terms of norms

$$|a(u,v)| \leqslant \int_\Omega \mathrm{d}\Omega |\vec{\nabla} u \cdot \vec{\nabla} v| + |\lambda| \int_\Omega \mathrm{d}\Omega |uv| \leqslant \|\nabla u\|_{L^2} \|\nabla v\|_{L^2} + |\lambda| \|u\|_{L^2} \|v\|_{L^2}. \tag{20}$$

Applying the Cauchy–Schwarz inequality and performing some algebra yields:

$$|a(u,v)| \leqslant (1+\lambda) \left(\|\nabla u\|_{L^2}^2 + \|u\|_{L^2}^2 \right)^{1/2} \left(\|\nabla v\|_{L^2}^2 + \|v\|_{L^2}^2 \right)^{1/2} = (1+\lambda) \|u\|_{H^1(\Omega)} \|v\|_{H^1(\Omega)}. \tag{21}$$

We now see that $a(u,v)$ is bounded because

$$\frac{|a(u,v)|}{\|u\|_{H^1(\Omega)} \|v\|_{H^1(\Omega)}} \leqslant (1+\lambda) < \infty \tag{22}$$

for all non-zero u and v.

The next step is to prove that a is coercive:

$$a(u,u) = \int_\Omega \mathrm{d}\Omega \vec{\nabla} u \cdot \vec{\nabla} u + \lambda \int_\Omega \mathrm{d}\Omega (u)^2 = \|\nabla u\|_{L^2}^2 + \lambda \|u\|_{L^2}^2 \geqslant \alpha \left\{ \|\nabla u\|_{L^2}^2 + \|u\|_{L^2}^2 \right\}, \tag{23}$$

or

$$a(u,u) \geqslant \alpha \|u\|_{H^1(\Omega)}^2, \tag{24}$$

where $\alpha \equiv \min(1,\lambda)$. Thus, as long as $\sigma/D > 0$, a is coercive.

The final step is to prove that $S(v)$ is bounded:

$$|S(v)| = \int_\Omega \mathrm{d}\Omega |v||f| \leqslant \|f\|_{L^2} \|v\|_{L^2} \Rightarrow \sup_{v \neq 0} \left\{ \frac{|S(v)|}{\|v\|_{L^2(\Omega)}} \right\} \leqslant \|f\|_{L^2(\Omega)} < \infty. \tag{25}$$

Thus, $S(v)$ is bounded if the original source function is bounded in the L_2 norm. For our problems of interest this is always true. We conclude that the Galerkin PWL method yields a well-posed problem when applied to a diffusion equation with $\sigma/D > 0$.

3.2. Order of accuracy as mesh is refined

By the Bramble–Hilbert lemma, we know that a discretization utilizing the standard linear basis functions on a tetrahedral mesh will have a second-order convergence rate in the L_2 norm [9]. We can further prove that the PWL method will have a second-order convergence rate if we can prove the difference between the standard interpolation:

$$I_h u = \sum_{j\in h} t_j u(\vec{r}_j) + \sum_{f\in h} t_{\mathrm{f}} u(\vec{r}_{\mathrm{f}}) + t_{\mathrm{z}} u(\vec{r}_{\mathrm{z}}) \tag{26}$$

and the PWL interpolation:

$$\widetilde{I}_h u = \sum_{j\in h} t_j u(\vec{r}_j) + \sum_{f\in h} t_{\mathrm{f}} \sum_{i\in f} \beta_{f,i} u(\vec{r}_i) + t_{\mathrm{z}} \sum_{j\in h} \alpha_j u(\vec{r}_j) \tag{27}$$

is also second-order. The difference between Eqs. (27) and (26) is

$$\widetilde{I}_h u - I_h u = \sum_{f\in h} t_{\mathrm{f}}^L \left(\sum_{i\in f} \beta_{f,i} u(\vec{r}_i) - u(\vec{r}_{\mathrm{f}}) \right) + t_{\mathrm{z}}^L \left(\sum_{j\in h} \alpha_j u(\vec{r}_j) - u(\vec{r}_{\mathrm{z}}) \right), \tag{28}$$

which will be second-order if

$$\sum_{i\in f} \beta_{f,i} u(\vec{r}_i) - u(\vec{r}_{\mathrm{f}}) = \mathrm{O}(h^2) \tag{29}$$

and

$$\sum_{j\in h} \alpha_j u(\vec{r}_j) - u(\vec{r}_{\mathrm{z}}) = \mathrm{O}(h^2). \tag{30}$$

We introduce Taylor series expansions of $u(\vec{r}_i)$ about point $\vec{r}_{\mathrm{f}}$ and of $u(\vec{r}_j)$ about point $\vec{r}_{\mathrm{z}}$:

$$\sum_{i\in f} \beta_{f,i} u(\vec{r}_i) - u(\vec{r}_{\mathrm{f}}) = \left(\sum_{i\in f} \beta_{f,i} - 1 \right) u(\vec{r}_{\mathrm{f}}) + \left(\sum_{i\in f} \beta_{f,i} (\vec{r}_i - \vec{r}_{\mathrm{f}}) \right) \cdot \nabla u(\vec{r}_{\mathrm{f}}) + \mathrm{O}(h^2) \tag{31}$$

and

$$\sum_{j\in h} \alpha_j u(\vec{r}_j) - u(\vec{r}_{\mathrm{z}}) = \left(\sum_{i\in f} a_j - 1 \right) u(\vec{r}_{\mathrm{z}}) + \left(\sum_{i\in f} a_j (\vec{r}_j - \vec{r}_{\mathrm{z}}) \right) \cdot \nabla u(\vec{r}_{\mathrm{z}}) + \mathrm{O}(h^2). \tag{32}$$

The summation terms on the right-hand sides vanish if for every face we have

$$\sum_{i\in f} \beta_{f,i} = 1 \quad \text{and} \quad \sum_{i\in f} \beta_{f,i} (\vec{r}_i - \vec{r}_{\mathrm{f}}) = 0, \tag{33}$$

and for every cell we have

$$\sum_{j\in h} \alpha_j = 1 \quad \text{and} \quad \sum_{j\in h} \alpha_j (\vec{r}_j - \vec{r}_{\mathrm{z}}) = 0. \tag{34}$$

These are in fact the equations that the PWL method uses to determine its cell and face midpoints and its basis functions. Thus, we expect the PWL solution to converge like $\mathrm{O}(h^2)$ in the L_2 norm.

3.3. Modal analysis and comparison of methods

We have also analyzed a simple test problem: infinite medium, 2D, rectangular cells, constant material properties, uniform mesh spacings. From this test problem we can use a simple mode analysis to determine how various methods' solutions compare with the analytic solution and with each other.

For this problem, the analytic solution of the diffusion equation can be determined for a source that can be written in terms of Fourier modes. The 2D diffusion equation is

$$-D \left[\frac{\partial^2 \phi(\vec{r})}{\partial x^2} + \frac{\partial^2 \phi(\vec{r})}{\partial y^2} \right] + \sigma_a \phi(\vec{r}) = S(\vec{r}). \tag{35}$$

The source can be expanded as

$$S(\vec{r}) = \int_{-\infty}^{\infty} \mathrm{d}w_y \int_{-\infty}^{\infty} \mathrm{d}w_x S_{\vec{w}} \exp(\mathrm{i}\vec{w} \cdot \vec{r}). \tag{36}$$

The solution can also be expanded

$$\phi(\vec{r}) = \int_{-\infty}^{\infty} \mathrm{d}w_y \int_{-\infty}^{\infty} \mathrm{d}w_x \phi_{\vec{w}} \exp(\mathrm{i}\vec{w} \cdot \vec{r}). \tag{37}$$

If we substitute Eqs. (36) and (37) into Eq. (35) and perform some algebra, we find that a given mode of the solution is independent of other modes and satisfies:

$$\phi_{\vec{w}} = \frac{S_{\vec{w}}}{D\|w\|^2 + \sigma_a}. \tag{38}$$

This analysis can also be applied to solutions of discretized diffusion equations. We have applied this to five discretization methods: lumped PWL (LPWL), unlumped PWL (UPWL), Palmer's method, lumped bilinear continuous FEM (LBL) and unlumped bilinear continuous FEM (UBL). After extensive but straightforward algebra we find that each method results in a solution of the form:

$$\phi_{\vec{w}} = \frac{S_{\vec{w}}}{D\{w_x^2 f_{\text{method}}(\theta_x, \theta_y) + w_y^2 f_{\text{method}}(\theta_y, \theta_x)\} + \sigma_a}, \tag{39}$$

where $\theta_x = w_x \Delta x$ and $\theta_y = w_y \Delta y$. Note that if the f factors were unity, the solution would be identical to the analytic solution. Also note that there are two different f factors in Eq. (39): the f function for the given method with the arguments in different orders. The f factors for each method are

$$f_{\text{LPWL}}(\theta_x, \theta_y) = \left[2\left(\frac{1-\cos(\theta_x)}{\theta_x^2}\right)\right]\left[\frac{3+\cos(\theta_y)}{4}\right], \tag{40}$$

$$f_{\text{UPWL}}(\theta_x, \theta_y) = \left[2\frac{1-\cos(\theta_x)}{\theta_x^2}\right]\left[\frac{3}{1+[1+\cos(\theta_x)]\frac{5+3\cos(\theta_y)}{6+2\cos(\theta_y)}}\right], \tag{41}$$

$$f_{\text{Palmer}}(\theta_x, \theta_y) = 2\left[\frac{1-\cos(\theta_x)}{\theta_x^2}\right], \tag{42}$$

$$f_{\text{LBL}}(\theta_x, \theta_y) = \left[2\left(\frac{1-\cos(\theta_x)}{\theta_x^2}\right)\right]\left[\left(\frac{2+\cos(\theta_y)}{3}\right)\right] \tag{43}$$

and

$$f_{\text{UBL}}(\theta_x, \theta_y) = \left[2\left(\frac{1-\cos(\theta_x)}{\theta_x^2}\right)\right]\left[\left(\frac{3}{2+\cos(\theta_x)}\right)\right]. \tag{44}$$

Each of these factors approaches unity in the fine-mesh limit ($\theta_x \to 0$ and $\theta_y \to 0$). We define an error for each method as

$$\varepsilon_{\text{method}} = |1 - f_{\text{method}}|. \tag{45}$$

The analysis shows that solution accuracy depends not only on the mesh size, which is expected, but also on the "modes" that are present in the source. If a problem has a non-smooth source, then high-wavenumber modes (large w values) are required to model the source. For this reason, to obtain accurate numerical results the mesh must resolve the wave numbers required to model any non-smooth sources.

Figs. 5–9 show plots of $\varepsilon_{\text{method}}(\theta_x, \theta_y)$ for each method. Because Palmer's and UBL's ε's depend on only one θ-variable, we have included a plot of both errors in Fig. 10.

From these equations and figures it is easy to see that Palmer's method's f factors will always be closer or as close to unity as the f factors of both the lumped PWL and lumped BL methods. In addition, the f values monotonically decrease from a value of unity as the problems move farther from the fine-mesh limit. As a result, for simple homogeneous problems on rectangular grids we expect Palmer's method to be slightly more accurate than the lumped FEMs for single-mode problems. This result is interesting because we anticipated that Galerkin finite element methods would be more accurate than Petrov–Galerkin finite element methods

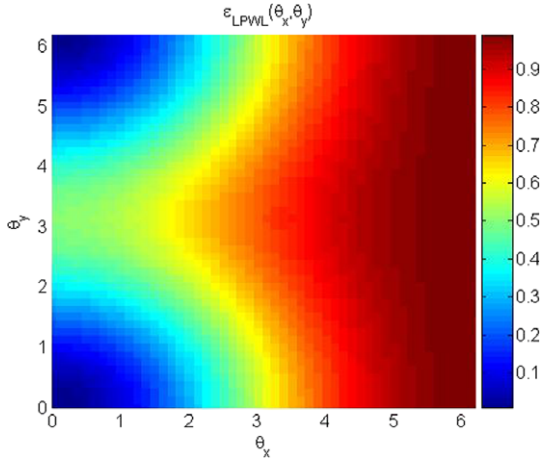

Fig. 5. Error for lumped PWL.

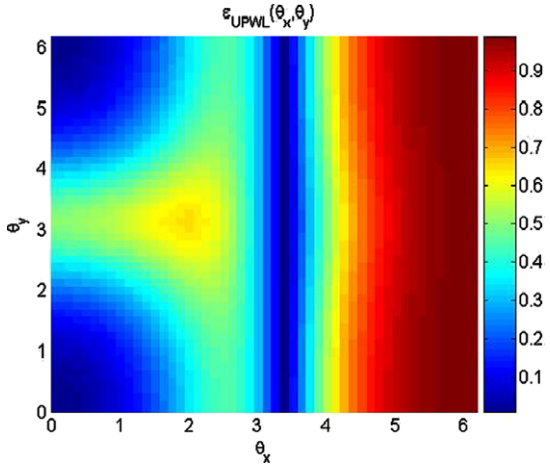

Fig. 6. Error for unlumped PWL.

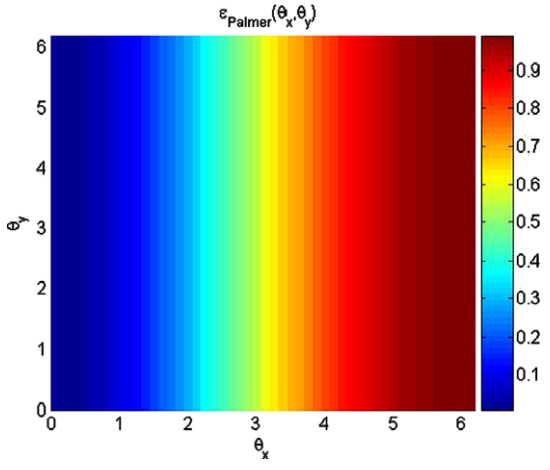

Fig. 7. Error for Palmer's method.

for discretizing the diffusion operator. When we "unlump" the FEMs, the f factors in the unlumped cases no longer monotonically decrease with increasing cell size. They become larger than unity, and then begin to decrease as the mesh size moves away from the fine-mesh limit. Furthermore, the unlumped FEM f values appear to stay closer to one for a larger range of θs. From this result, we conclude that we gain some accuracy if we do not lump (or lose accuracy when we lump) the FEMs and incur non-monotonic convergence away from the fine-mesh limit. Finally, we notice that the behaviors of the PWL and BL methods are strikingly similar, although the accuracy of the lumped PWL method is always better than the accuracy of the lumped BL method for a given mode, and the accuracy of unlumped BL is always slightly better than the accuracy of unlumped PWL for a given mode. This similarity indicates that the discontinuities in the derivatives of the PWL basis functions do not have a significant impact on the accuracy of the method.

4. Results

4.1. Accuracy

To test our implementation of the Galerkin PWL method as well as the prediction of perfection for linear solutions, we consider a three-dimensional problem with a linear solution that varies only in x. This problem has no source, no absorption, reflecting boundary conditions for the z and y dimensions, and Dirichlét boundary conditions of $E(0,y,z)=0$ and $E(1,y,z)=1$. Figs. 11 and 12 show contour plots of this solution generated by our Galerkin PWL method on a random mesh and a "Z-mesh" [10]. From these plots (and many similar ones), we conclude that the PWL method does reproduce the exact linear solution. This property is also attained by Palmer's method.

A Z-mesh problem with a linear solution in x, y and z was also run to show that the method produces the linear solution on a difficult mesh in all dimensions. This test problem had absorption, a linear source, and applied Dirichlét boundary conditions that enforced a linear solution on each face. Solution contours should be straight diagonal lines, and they are, as we see in Fig. 13.

There is considerable interest in discretizations on grids with "hanging nodes," such as the grids produced by many adaptive mesh refinement (AMR) algorithms. A coarse "brick" cell adjacent to four finer "brick"

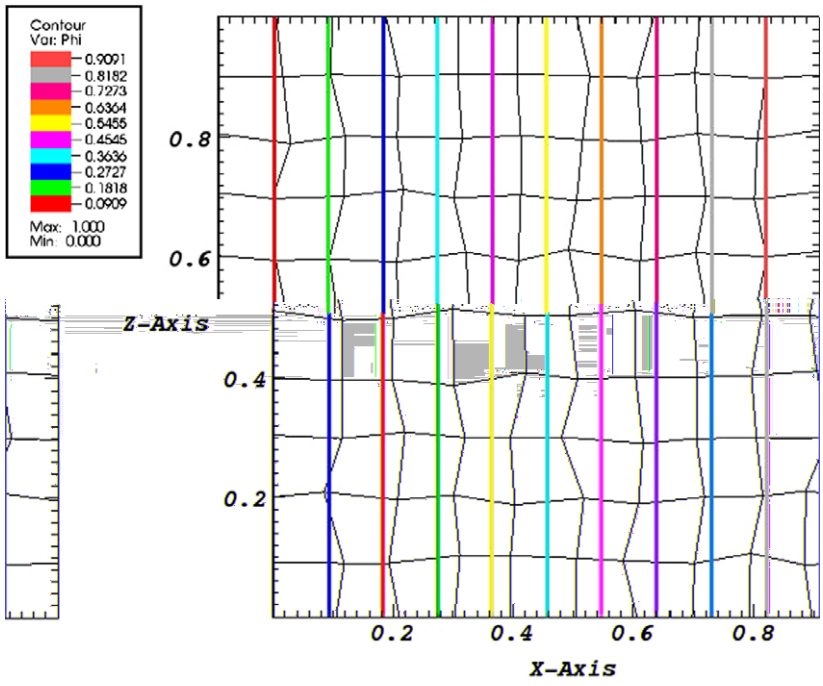

Fig. 11. Contour plot of a 1D linear solution on a random mesh at $y = 0.75$. (Solution is the same on other y-planes, as it should be.)

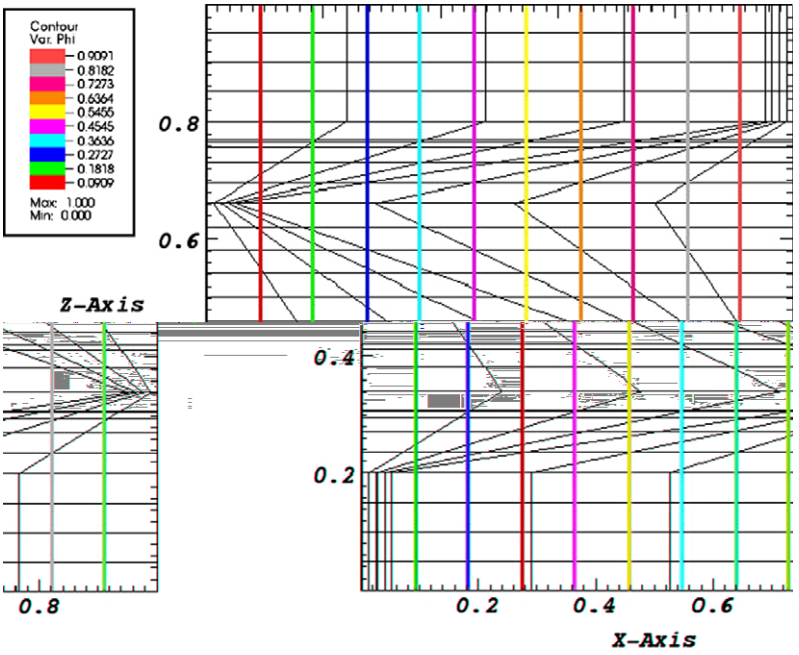

Fig. 12. Contour plot of a 1D linear solution on a Z-mesh at $y = 0.75$. (Solution is the same on other y-planes, as it should be.)

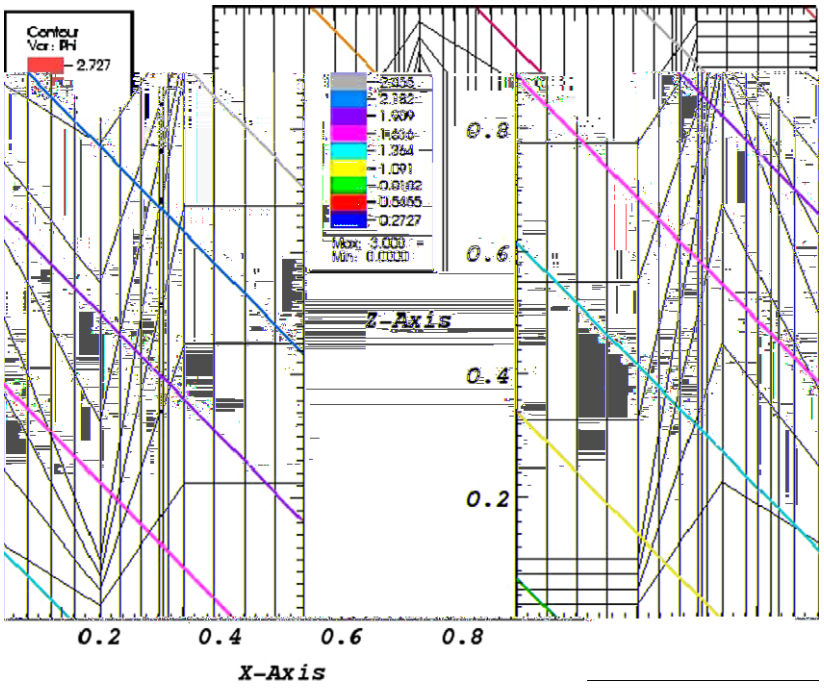

Fig. 13. Contour plot of 3D linear solution on a Z-mesh, slice at $y = 0.75$.

cells is usually viewed as a brick with a hanging node on one face and four hanging nodes on four edges, but it could also be viewed as a polyhedron with 9 faces (because one of the six "brick" faces has become four smaller faces). In the latter view, there are 180-degree angles between adjacent faces, which could cause difficulties for some finite element methods. For example, Wachspress functions become singular for such polyhedra, which Wachspress calls "ill-posed." However, our analysis of the PWL method suggests that it will behave

well on such hanging node grids. Our first numerical test of this uses a grid with two levels of refinement on a problem with a linear solution. We show the result of this test problem in Fig. 14. In the fifth column of zones from the left, some of the mesh lines are missing in this plot because the visualization software we used did not render the hanging nodes correctly. The solution contour lines do in fact extend straight across this set of zones. Thus, we see that 180-degree angles do not cause PWL to lose its property of capturing linear solutions exactly. A second hanging node test problem below will address PWL behavior for more complicated solutions.

The next set of problems tests the convergence rate of both the PWL method and Palmer's method on a series of random meshes, and on orthogonal meshes. (Each random mesh was generated by randomly perturbing each non-boundary vertex of an orthogonal mesh.) One test measures the convergence rate for a problem with a known one-dimensional quartic solution. Palmer used this same problem to test the convergence rate of his finite-volume method [1]. This problem has no absorption, a quadratic source, and Dirichlét boundary conditions of $E(0,y,z)=0$ and $E(1,y,z)=1$. The results from this test are found in Fig. 15.

A second test problem was developed to further test the convergence rate. This problem includes absorption, has no source, and Dirichlét boundary conditions of $E(0,y,z)=1$ and $E(1,y,z)=0$. It has an exponential solution. The results from this test are also found in Fig. 15. The error norm is calculated by taking the L_2 norm of the vector of the exact solution minus the calculated solution. The convergence rate of the methods is determined by the slopes of the lines in Fig. 15. If the slope is two on the log–log plot, the method has a second-order convergence rate, which means that the error in the solution gets decreased by a factor of four when the mesh is refined by a factor of two. In Fig. 15 we plot a reference line with a slope of exactly two to compare the results of the numerical tests. We also plot errors from the two test problems described previously. The results from the quartic solution problem appear above the black reference line. These results show that for this test problem, not much accuracy is lost when the mesh changes from brick to random. The results from the exponential solution problem appear below the reference line. These lines represent the convergence rates of PWL and Palmer's method on random meshes for an exponential solution, and PWL on brick meshes for an exponential solution. These results show that for this test problem, the methods lose about a factor of

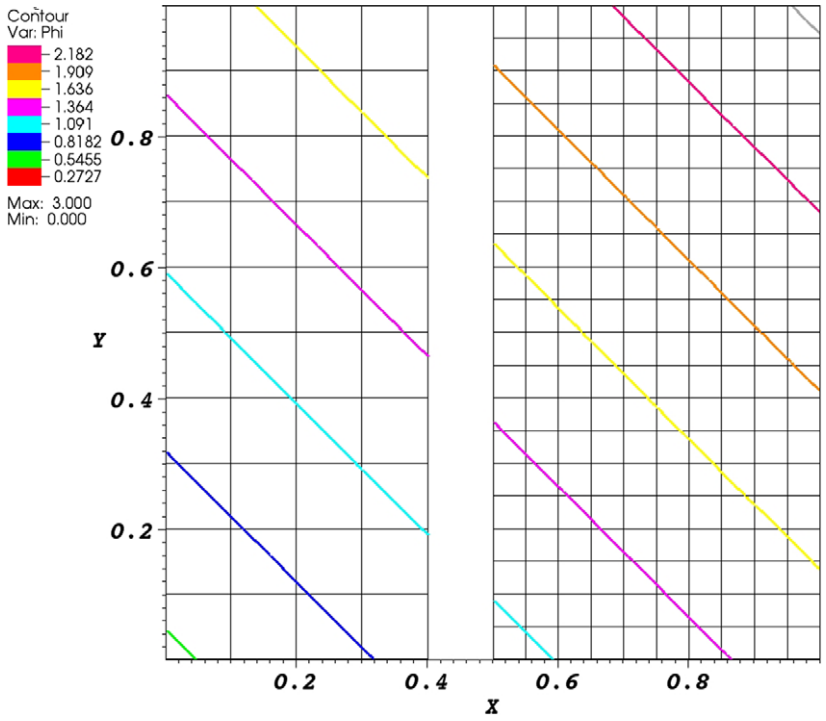

Fig. 14. Contour plot of 3D linear solution on a mesh with hanging nodes, slice at $z=0.5$. (Our plotting software did not render the solution or grid in the column of coarse cells at the interface.)

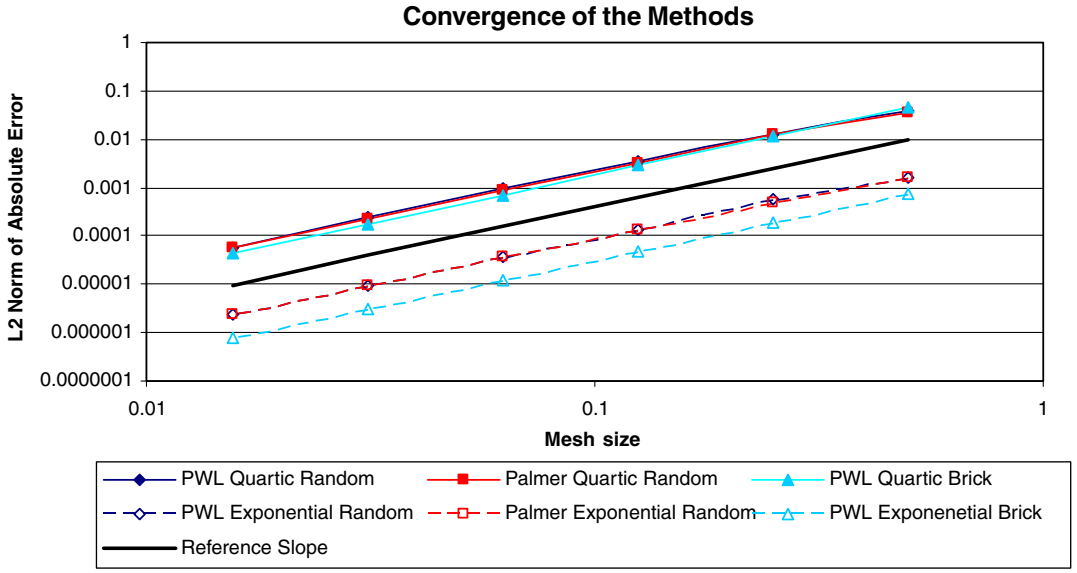

Fig. 15. Convergence rates of Palmer's method and PWL on various test problems.

three in accuracy when the mesh is changed from a brick mesh to a random mesh. In general, both methods show second-order accuracy and have the same magnitude of error for both the quartic problem and the exponential problem.

We also ran a quartic solution test problem on a mesh with hanging nodes. The analytic solution is $[(x+y+z)/3]^4$. The PWL solution is shown in Fig. 16. The values obtained at the vertices are very nearly exact throughout the problem, which is a very strong result. (There are kinks in the within-cell contours because the plotting software divides each rectangle into two triangles and then linearly interpolates on each triangle. For this problem the software chose to split along the diagonals from lower left to upper right; the other choice would not produce kinks.) The PWL solution is well-behaved, with no hint of difficulty treating the coarse cells at a refined interface as polyhedra with 180-degree angles between faces. Because of our results and analyses, we believe that the PWL method is an effective spatial discretizations for AMR-type grids. We do not show results, but we find that Palmer's method also works well on such grids.

We have analyzed the Galerkin PWL method in the limit of high aspect ratios on two-dimensional orthogonal grids and found that the signs of the off-diagonal elements in the diffusion matrix will change at certain ratios of Δx and Δy. For $(\Delta x/\Delta y)^2 < 1/3$, the sign change occurs for the vertices that are above and below the central vertex. For $(\Delta y/\Delta x)^2 < 1/3$, the sign change occurs for the vertices to the left and right of the central vertex. Thus, for problems with cells of high-aspect-ratio, the coefficient matrix is no longer an "M-matrix." This raises the possibility that its inverse could have negative elements, which in turn raises the possibility that in some problems the method could produce unphysical oscillations and/or negative solutions. To test this we ran a problem on an orthogonal mesh with 64 cells of the 1024 total cells having 1000 to 1 aspect ratios $(\Delta y/\Delta x)$. These cells were contiguous, and inserted into the problem at $x = 0.375$ on a cubical domain of unit width. The test problem had Dirichlét boundary conditions of $E(0,y,z) = 0$, $E(1,y,z) = 0$, $E(x,0,z) = 0$ and $E(x,1,z) = 0$, and reflecting boundary conditions in the z-direction. The source in this problem is a "point source" inserted into the problem at only one vertex in the middle of the region containing cells with high-aspect-ratios. The plot of the PWL solution is shown for an equally spaced mesh in Fig. 17 and a mesh with high-aspect-ratio cells in Fig. 18.

These plots show just a slice of the problem. The slice was taken at the value of z where the solution reaches its maximum.

The presence of the high-aspect-ratio cells does not affect the solution significantly. In particular, despite the singular source, there are no unphysical oscillations or negative values in the PWL solution, which indicates that the even though the matrix is not an "M-matrix" its inverse has no negative values. This positive result

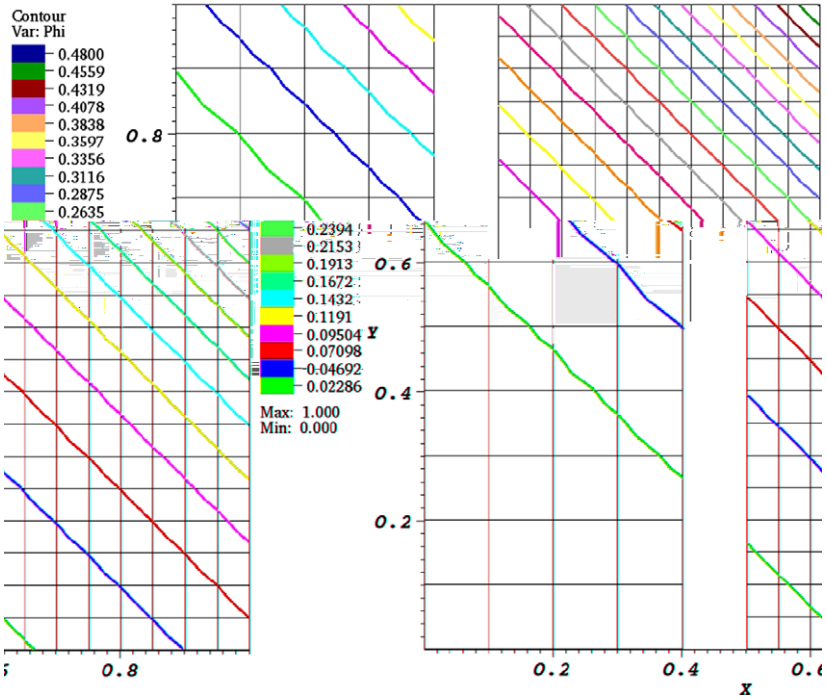

Fig. 16. Contour plot of 3D quartic solution of grid with hanging nodes, slice at $z = 0.5$. (Our plotting software did not render the solution in the coarse cells at the interface.)

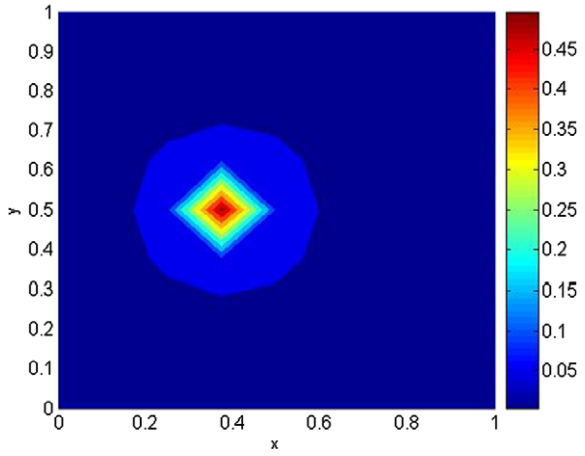

Fig. 17. Contour plot at $z = 0.5$ of the point source problem for an equally spaced mesh with the source at $x = 0.375$ and $y = 0.5$.

is somewhat surprising. The problems with uniform and non-uniform grids have the same source strength, which is input into both problems at a single node with the same coordinates. The magnitude of the solution is slightly larger (0.6%) for the problem with the high-aspect-ratio cells, but we attribute this small difference to the finer mesh spacing near the source. We plan further analysis and testing, including problems with distorted grids, to better understand this unexpectedly robust behavior in the presence of high aspect ratios.

4.2. Efficiency

Because PWL produces an SPD matrix, we can use the Conjugate Gradient (CG) method to solve the matrix system. Palmer's method must be solved using an asymmetric solver such as GMRES. We expect that

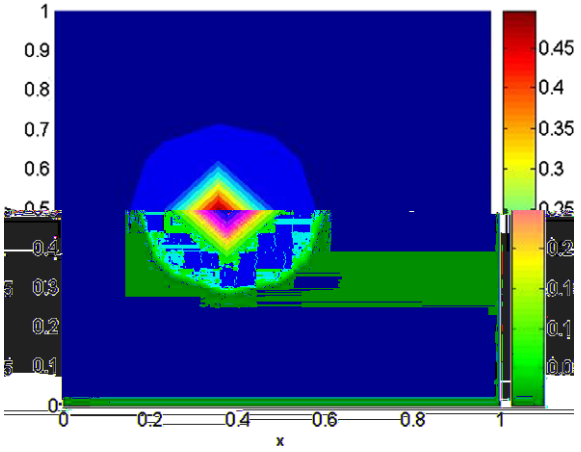

Fig. 18. Contour plot at $z = 0.5$ of the point source problem for a mesh with high-aspect-ratio zones with the source at $x = 0.375$ and $y = 0.5$.

CG will be more efficient, and we test this conjecture on a time-dependent "tophat" problem, with the radiation diffusion equation coupled to an energy-balance equation for the material (which the material temperature must satisfy). The tophat problem is a two-material problem, with a high-density region surrounding a low-density region, as shown in Fig. 19. The low-density region forms a crooked pipe through which radiation will flow, with a shape resembling a tophat. While the details are not important for our purposes here, we note that the material opacities are temperature-dependent and the radiation source is a Planckian at the material temperature.

The boundary conditions and geometry for this problem are set up to simulate an axisymmetric problem on a 3D Cartesian coordinate system. The problem domain is a wedge in the XY plane, going from a knife-edge on axis to finite thickness at the outer part of the cylinder. The large flat faces are reflecting, the outer-cylinder boundary is vacuum, the rightmost triangular surface is vacuum, and there is incident radiation on the leftmost triangular face. In more detail, the incoming intensity is specified on the left boundary only along the low-density material (the pipe entrance), corresponding to a Planckian intensity at $kT = 0.3$ energy units. Everywhere else on this surface, the value of the boundary condition is vacuum. The initial material temperature is $kT = 0.05$ everywhere in the domain, and the simulation is run for 1000 units of time. A few plots of the simulation results are shown in Fig. 20. These plots were generated using PWL as the diffusion solver. As expected, the radiation flows through the thin region and also eventually "eats" its way into the thick region. This is interesting in itself, but our purpose here is simply to illustrate the performance of CG and GMRES solvers.

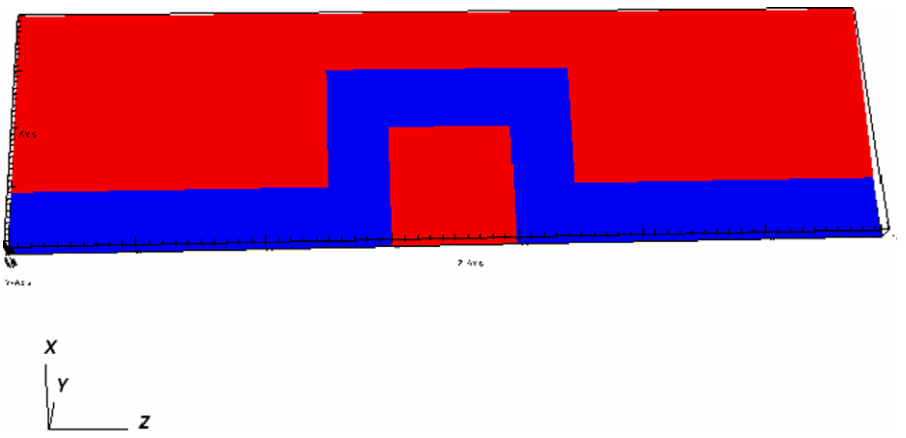

Fig. 19. The material densities of the tophat problem.

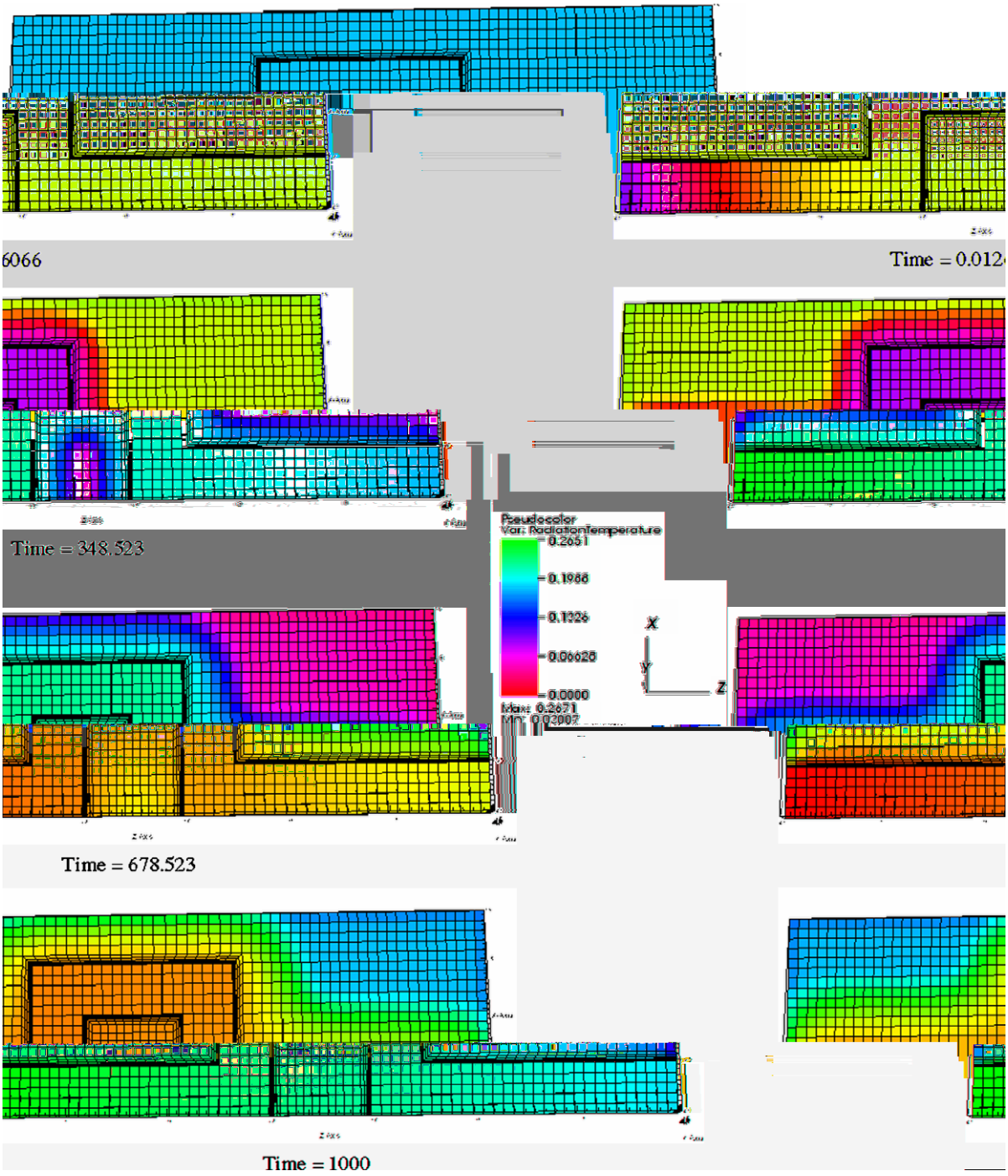

Fig. 20. The radiation temperature in the tophat problem shown at different time steps.

We compared the effectiveness of both iterative methods (GMRES for Palmer and PWL, and CG for PWL) by comparing the number of iterations required to invert the matrix for each reported time step. The preconditioner used for all linear solvers was Algebraic Multigrid.

The results of these calculations, shown in Fig. 21, show that CG for PWL requires a factor of three fewer iterations than does GMRES for Palmer's method. (Also, in general GMRES applied to PWL requires

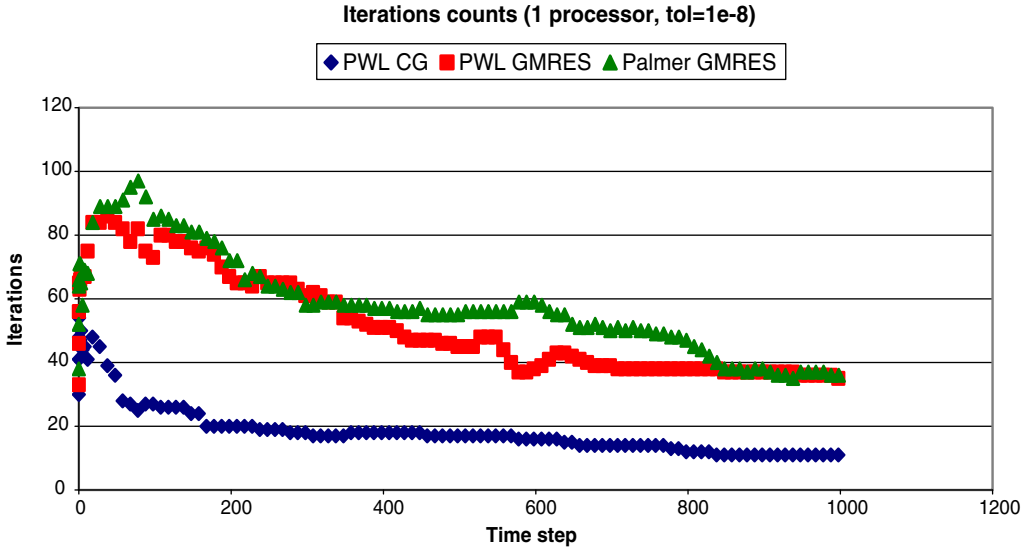

Fig. 21. Linear solver comparisons for PWL and Palmer's method for 1 processor.

slightly fewer iterations than GMRES applied to Palmer's method, which indicates that the PWL matrix is slightly better conditioned than that of Palmer's method.) We further note that in a parallel computing environment, CG has even more advantages over GMRES, because it requires fewer inner products per iteration, and each inner product requires global communication. The combination of reduced storage for the matrix, far fewer iterations, reduced storage of solution-length vectors, and fewer inner products per iteration should make the Galerkin PWL method substantially more efficient than Palmer's method.

5. Conclusions

Our tests show that the Galerkin PWL finite element method applied to the radiation diffusion equation on arbitrary polyhedral meshes has great potential for computational improvements over previous methods. As we had hoped, the PWL method produces results and behaviors almost identical to those of Palmer's method. Palmer's method has a slight theoretical advantage on orthogonal ("brick") grids in that it generates a highly robust 7-point discretization whereas PWL generates full 27-point coupling. However, our tests on problems with very high-aspect-ratio cells did not uncover any poor PWL behavior. Further, the PWL coefficient matrix is SPD, which allows for less storage and potentially more computationally efficient solutions. We conclude that the Galerkin PWL method is a very attractive option for solving diffusion problems on unstructured grids.

Acknowledgments

We thank Jean-Luc Guermond for many helpful discussions concerning the Lax-Milgram and Bramble–Hilbert Lemmas. The research described here was supported in part under the auspices of the US Department of Energy at the Lawrence Livermore National Laboratory under Contract No. W-7405-ENG-48. The work of the first author was supported by the US Department of Energy Computational Sciences Graduate Fellowship Program.

Appendix I. Polyhedral cell definitions

We have used the term arbitrary polyhedra to describe the types of three-dimensional cells over which we discretize the diffusion equation. Our definition of a polyhedral cell is a volume enclosed by an arbitrary number of faces, each determined by an arbitrary number (3 or more) of vertices. If a face has four or more ver-

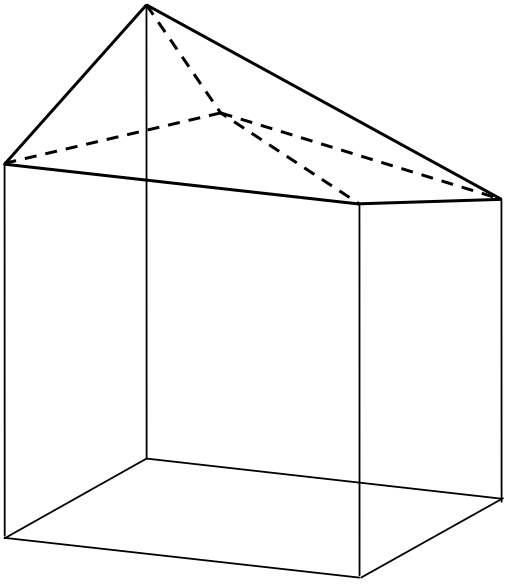

Fig. I.1. Faceted face of a hexahedral cell.

tices, it is possible that these vertices are non-coplanar and thus the "face" is not a plane. Many methods exist to construct a representation of a "face" that has non-coplanar vertices. Some methods create curved surfaces for faces; our method does not. Instead, we divide the face into triangular "facets" about a face center point.

In order to create our face representation, we first select a face center point, which is some linear combination of the vertices in the face, given by

$$\vec{r}_{\mathrm{f}} \equiv \text{face midpoint} = \sum_{j \,\mathrm{at}\, f} \beta_{f,j} \vec{r}_j, \tag{I.1}$$

where $\beta_{f,j}$ is chosen to be the same as the values for the PWL basis functions. For the problems shown in this paper, we choose these β values to be equal to $1/N$ for all N vertices of the face. We then facet our face about this point, so that the face becomes a collection of triangular planes. Because the β values are chosen the same way in faceting the face as in developing the PWL basis functions, the sides created by this face are exactly the same as the sides over which the basis functions are defined. (Recall that a side is defined by two adjacent vertices in a cell, the cell-center point, and the face center point in which corresponds to the face that contains both vertices). Fig. I.1 shows a hexahedral cell whose top face has four non-coplanar vertices. The facets of this face are drawn with dashed lines.

In the PWL method, a hexahedral cell such as the one depicted above involves only eight unknowns, one for each vertex of the cell. There are no unknowns at the face or zone center points. If we facet all of the faces in a general hexahedral cell, it can be viewed as a polyhedron with 24 faces and 14 vertices. Such a cell could be treated as a 14-vertex polyhedron with unknowns at all 14 vertices; however, by treating it as a hexahedron with faceted faces, we avoid the introduction of face centered unknowns, considerably reducing computational complexity.

We remark that our procedure for "faceting" non-planar faces produces "side" subcells that are simple tetrahedra with flat faces. As a result, computing PWL matrix elements involves integrations only on ordinary tetrahedral, which keeps the implementation simple.

References

[1] T.S. Palmer, Discretizing the diffusion equation on unstructured polygonal meshes in two dimensions, Ann. Nucl. Energy 28 (2000) 1851–1880.

[2] T.S. Palmer, A point-centered diffusion differencing for unstructured meshes in 3-D, in: Proceedings of International Conference in Mathematics and Computations, Reactor Physics and Environmental Analyses, Portland, OR, April 30–May 4, 1995, vol. 2, pp. 897–905.

[3] E.L. Wachspress, A Rational Finite Element Basis, Academic Press, New York, 1975.
[4] G.G. Davidson, T.S. Palmer, Finite element diffusion on arbitrary quadrilaterals using rational basis functions, Trans. Am. Nucl. Soc. 87 (2002).
[5] H.G. Stone, M.L. Adams, A piecewise linear finite element basis with application to particle transport, in: Nuclear Mathematical and Computational Sciences Meeting, Gatlinburg, TN, CD-ROM, April 6–11, 2003.
[6] J.E. Morel, A 3-D cell-centered diffusion discretization for arbitrary polyhedral meshes, Los Alamos National Laboratory Research Note, CCS-4:02-40(U), 2002.
[7] Yu. Kuznetsov, K. Lipnikov, M. Shashkov, Mimetic finite difference method on polygonal meshes, Los Alamos National Laboratory Report, LA-UR-03-7608, 2003.
[8] M.L. Adams, P.F. Nowak, Asymptotic analysis of a method for time- and frequency-dependent radiative transfer, J. Comput. Phys. 146 (1998) 366–403.
[9] A. Ern, J.L. Guermond, Theory and Practice of Finite Elements, Springer-Verlag, New York, 2004.
[10] D.S. Kershaw, Differencing of the diffusion equation in lagrangian hydrodynamic codes, J. Comput. Phys. 39 (1981) 375.